PHYSICAL REVIEW B VOLUME 21, NUMBER 8 15 APRIL 1980

Nitrogen states in Ga(As,P) and the long-range, short-range model: A systematic study

George G. Kleiman and M. Fracastoro-Decker
Instituto de Física, Universidade Estadual de Campinas, 13.100-Campinas, São Paulo, Brazil
(Received 9 April 1979)

The long-range, short-range model of the nitrogen isoelectronic impurity in Ga(As,P) is discussed in terms of the results of recent photoluminescence and lifetime measurements. The predictions of the theory are shown to depend sensitively upon the strength of the coupling among the states produced separately by the long- and short-range parts of the potential: The strength of the coupling reflects the specific model of potential used in all cases treated. Strong coupling yields theoretical energies whose general composition dependence mirrors the features of the data. The effect of consideration of the L-conduction-band minima is smaller. Determination of potential parameters from experimental energies indicates a range ~ 20–25 Å. Luminescence calculations require an accurate treatment of the continuum contribution. Predictions of the theory are in good agreement with available data. Inclusion of L indicates the existence of an excited nitrogen state in GaP. No internal inconsistencies in the theory are found.

I. INTRODUCTION

Because it is strongly luminescent even in indirect III-V mixed-crystal alloys [particularly Ga(As, P)], the isoelectronic impurity nitrogen has attracted wide interest in its optical properties.[1] These properties have permitted commercial production of yellow Ga(As, P):N light-emitting diodes,[1] for instance. More fundamentally, nitrogen in Ga(As, P) has been considered[1,2] to be a classic example of a short-range impurity, as opposed to the common hydrogenic donors and acceptors in semiconductors.

More recent experimental data[3-10] indicate that the nitrogen potential in Ga(As, P) is more complicated than in the simple short-range Koster-Slater[11] model treated in previous work.[2,12-21] Instead of the single state predicted by the Koster-Slater model,[2,11-18] more than one state associated with single nitrogen sites has been experimentally identified.[3-10] The energy E_{N_X} of the lowest experimental line N_X decreases monotonically with decreasing x, the mole fraction of phosphorus, and is associated with the X conduction-band minimum,[22] as demonstrated by pressure measurements.[5] The energy E_{N_Γ} of the next higher line N_Γ follows[5] the Γ minimum for $x \lesssim 0.42$, bends over for $x \simeq 0.42$, and then follows the X minimum for $x \gtrsim 0.42$ until $x \simeq 0.47$; there has been no observation of N_Γ for $x \gtrsim 0.47$.

Photoluminescence data for as-grown Ga(As, P):N are illustrated in Fig. 1.[10,23] In addition to the two states discussed above, these data manifest the existence[10] of a third state N_Γ', which had been predicted theoretically.[6,24] Corresponding data[25] for samples in which nitrogen ions were implanted seem to show no evidence of N_Γ'. This discrepancy may be the result of the difference between as-grown and ion-implanted material.

Interpretations of features of the data in limited ranges of x have been made in terms of the traditional models of impurity potentials: That is, either short-range models whose electronic states are nonlocal in $\vec{k}$ space, or long-range models whose states are localized in $\vec{k}$ space about conduction-band minima (i.e., the effective-mass approximation holds).[19,20] Attempts to interpret the single N_X state observed for $x \gtrsim 0.47$ in terms of the influence of the newly measured[19,20] x dependence of the L conduction-band minimum upon a two-level version of the Koster-Slater model produced good agreement with experimental data.[5] It was demonstrated,[21,25] however, that uncertainties in the band structure (or density of states) vitiate the physical significance of any such agreement. A long-range model impurity potential, on the other hand, was exploited[4] to interpret the data for $0.30 \lesssim x \lesssim 0.42$, where N_Γ follows Γ and N_X follows X. Even though good agreement with experimental energies was again achieved,[4] this model localizes N_X about X in $\vec{k}$ space and cannot explain the strong luminescence of N_X, which implies large $\vec{k} = 0$ wave-function components.

It is clear from the foregoing discussion that the nitrogen potential must be intermediate between the short- and long-range limits in order to correspond to experiment. That is to say, it must have a short-range part to provide the large $\vec{k} = 0$ components and a more extended part to account for the multiple states observed.[3-10] It is equally clear that care must be taken to account for *all* the experimental features consistently from the model potential considered: Either considering only the strong luminescence and neglecting the description of the rest of the spectrum[19,20] or treating only the independent x dependences of N_Γ and N_X and neglecting the luminescence[4] leads to inconsistencies.

Two theories involving extended nitrogen poten-

tials have been proposed[6,24,25] to describe the data.[3-10] One[25] of these theories associates the nitrogen impurity with an intermediate-range extended part V_l as well as a short-range part V_s. More specifically, the strain field is presumed to induce an attractive impurity potential in the first shell of nitrogen nearest neighbors as well as at the nitrogen site. This model predicts *two* symmetric states (i.e., with large $\vec{k}=0$ probability amplitudes). In the calculations reported,[25] these states are decoupled and fitted independently to N_Γ and N_X near $x \cong 0.35$. The limited range of the potential causes neither of these states to be localized in $\vec{k}$ space about a conduction-band minimum. The association of one state (arising from the nitrogen site) with X and the other (arising from the shell) with Γ is, therefore, a result of fitting the data and is not an intrinsic consequence of the model.[25]

It would seem that this intermediate-range model[25] is consistent with experiments[25,26] on ion-implanted material as well as with conventional intuition regarding the problem. In a recent study,[27] however, it was demonstrated that the fundamental decoupling of the two states upon which all the subsequent calculations and predictions rest[25] is untenable: In fact, there are *no* parameters for which the energies calculated from this model can be fitted to the experimental data in Ga(As, P).[27]

These conclusions were extended to more general intermediate-range models[27] (i.e., restricted to finite regions of the crystal). From basic quantum-mechanical considerations, it was shown[27] that no monotonic potential of range less than 20–25 Å (i.e., no intermediate-range potential) is consistent with the experimental energies.

The other theory,[6,24] based upon an extended nitrogen potential, attributes a long-range potential V_l as well as the conventional short-range potential V_s to the nitrogen. The long-range potential is presumed to arise from deformation of the lattice induced by strains associated with the presence of nitrogen. To account for the data, the only property which is required of V_l is that it be strong enough to bind one state associated with X and one with Γ; the short-range potential V_s is presumed to produce a bound state which is delocalized in $\vec{k}$ space as in the conventional Koster-Slater picture. Since the observed lines are associated with eigenfunctions corresponding to $V = V_l + V_s$, the predictions of the theory can be interpreted[6,24] as arising from hybridization of the states associated with V_l and V_s separately and result from the *intrinsic nature of* V independent of specific values of potential parameters. These predictions are in agreement with all the general features of the data: That is, the theoretical energies display the same general x dependences as the experimental data in Fig. 1.

The physics of the luminescence of the states produced by this theory can be readily understood by appeal to the one-band, one-site Koster-Slater model of nitrogen.[2,12-18] The short-range of the potential causes an eigenstate to have components for all $\vec{k}$ within the first Brillouin zone (BZ). The state is derived from the conduction band of the perfect crystal so that one such component is proportional to the Bloch-function representation of the perfect-crystal Green's function, which is proportional to $[E_N - E_c(\vec{k})]^{-1}$, where E_N is the energy of the state and $E_c(\vec{k})$ is the conduction-band dispersion relation. Therefore the localized impurity state has strong $\vec{k}=0$ components (i.e., strong luminescence) even in indirect crystals, and this luminescence increases as $E_N \to E_c(\vec{k}=0) \equiv E_\Gamma$ (this increase incorporates the phenomenon of band-structure enhancement or BSE[2]).

Within the long-range, short-range model,[6,24] we can represent V_s by a Koster-Slater potential and again find that the momentum amplitudes are proportional to the Bloch representation of a Green's function. The Green's function in this case, however, involves not the conduction-band states but, rather, the eigenstates arising from the presence of V_l. This means that each of the eigenstates corresponding to $V_l + V_s$ has contributions from the strongly luminescent bound state produced by V_l associated with Γ as well as from the continuum states (which correspond to the ordinary Koster-Slater result). This model, therefore, gives rise naturally to multiple impurity states, all of which are strongly luminescent.

In earlier work,[6,24] the general consequences of the model were discussed and the results of simplified numerical calculations (in which only Γ and

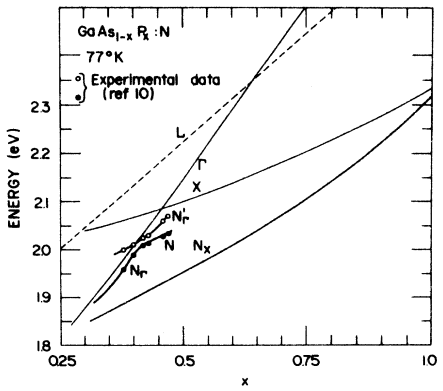

FIG. 1. Photoluminescence data indicating the concentration dependence of Γ, X, L and the peaks associated with electronic states of isolated nitrogen impurities in Ga(As, P) (after Refs. 10 and 23).

X were considered) were presented[24] in order to illustrate the degree of agreement with available experiment[5] which could be achieved. The quantitative agreement was adequate[6,8,24] considering the simplicity of the calculations. The potential parameters which were extracted[24] from experimental data were consistent with fundamental requirements: For instance, the radius of the square well used to model V_l was 20–25 Å in accord with the long-range nature of V_l (i.e., the effective-mass approximation is valid).

In view of the recent criticism[27] of intermediate-range models, however, it is interesting to inquire if the conclusions based upon the long-range model remain unchanged after a more complete numerical study [in which the effects of L (Refs. 19 and 20) are examined], or if there is, perhaps, an inconsistency which has escaped notice. Furthermore, criticisms apparently arising from the results of the early numerical applications[24] of the model have been leveled[25] against the supposed difficulty in reconciling this model with the conventional picture[2,12] of nitrogen in GaP, the presumed requirement of the theory that there be multiple bound states even for $x > 0.5$, and the seeming underestimation of the predicted N_X luminescence strength: It would be interesting to see if a strict numerical application of the theory could provide answers to these criticisms. Finally, the availability of a larger and more complete body of data[3-10,25,26] than that treated previously[24] makes it desirable to present the numerical results of a systematic study of the model in a form ready for comparison with data.

In this paper we report the results of such a study of the long-range, short-range model in its applications to Ga(As, P):N. This study is considerably more complete than that presented previously.[24] In Sec. II A we neglect the effect of L for the moment and examine the consequences of increasing the coupling between the states produced by V_l (which we model by a square well) and V_s separately and demonstrate that, in the more realistic case of strong coupling (as opposed to the weak coupling considered previously[24]), the states of $V_l + V_s$ exhibit all of the characteristics of the data in Fig. 1. In particular, the presence of strong coupling produces only one state in the gap for large x and there is no difficulty in relating the results for GaP with those for the alloy. In addition, we show that it is necessary to take into account the influence of V_l when calculating the continuum contribution to the $\vec{k} = 0$ momentum amplitudes instead of using only Bloch states for the continuum.[24] Finally, we show how inclusion of the effects of strong coupling changes the values of the parameters extracted from the data for this case and that these parameters are still consistent with both the fundamental restrictions of the model and the conventional picture of GaP:N.[2]

In Sec. II B we investigate the effects of both strong coupling and the inclusion of the large density of states associated with the L conduction-band minima upon the spectrum of states and the $\vec{k} = 0$ momentum amplitudes. Potential parameters extracted from the data in this case are also consistent with the long-range nature of the potential although the results for GaP suggest a modification of conventional[2] notions. We discuss comparison with experiment in Sec. III for the cases where L is considered and where it is not, and in Sec. IV we present the conclusions.

In brief, it appears that the long-range, short-range (or Kleiman[6,24]) model is the only one which describes all of the experimental data without internal inconsistencies. The consequences for other impurities in other semiconductors should be carefully investigated.

II. SYSTEMATICS OF THE LONG-RANGE SHORT-RANGE MODEL

A. Influence of strong coupling

In this part, we consider only the Γ and X minima, demonstrate the effects of increased coupling upon the states, and show that the parameters extracted from the data are consistent with the long-range nature of the potential. As in previous work,[6,24] we model the impurity potential by the sum of a short-range part V_s and a long-range part V_l. We employ the one-band, one-site Koster-Slater model[11-18] to represent the short-range part of the potential V_s, so that its matrix elements between Wannier states $|\vec{R}_m, s\rangle$ associated with lattice site $\vec{R}_m$ and band s are given by

$$\langle \vec{R}_m, t | V_s | \vec{R}_n, s \rangle = V_0 \delta_{mn} \delta_{m0} \delta_{st} \delta_{sc} , \tag{1}$$

where $\vec{R}_0 = 0$ denotes the impurity site, c represents the lowest conduction band, and V_0 is the Koster-Slater[11] parameter. Since we consider coupling to conduction-band states only, a bound state $|j\rangle$ can be written as

$$|j\rangle = \sum_m |\vec{R}_m, c\rangle \langle \vec{R}_m, c | j \rangle , \tag{2a}$$

where in the Koster-Slater approximation,

$$\langle \vec{R}_m, c | j \rangle = V_0 G(\vec{R}_m, \vec{R}_0, E_j) \langle \vec{R}_0, c | j \rangle . \tag{2b}$$

The quantity E_j is the energy eigenvalue of $|j\rangle$ and G is the retarded conduction-band Green's function in the Wannier representation, which obeys the following equation:

$$G(\vec{R}_m, \vec{R}_n, E) \equiv \sum_p \frac{f_p(\vec{R}_m) f_p^*(\vec{R}_n)}{E + i\delta - W_p} , \tag{2c}$$

$$[E_c(\vec{\nabla}/i)+V_l(\vec{r})-W_p]f_p(\vec{r})=0\,. \tag{2d}$$

The quantity $\delta \to 0^+$ in our treatment. Equation (2d) results[24] from the assumption that $V_l(\vec{r})$ is sufficiently slowly varying that the effective-mass approximation holds true [i.e., $\langle \vec{R}_m, c|V_l|\vec{R}_n, c\rangle \simeq V_l(\vec{R}_m)\delta_{mn}$], and we have made the extension to continuous $\vec{r}$ values instead of the discrete lattice points for which Eq. (2d) is strictly valid. We denote the energy eigenvalues of f_p as W_p and the star denotes complex conjugation.

The energy eigenvalues of $|j\rangle$ are given by the solutions of[24]

$$V_0\,\mathrm{Re}[G(0,0,E_j)]=1\,. \tag{3a}$$

Normalization of the wave function to unity yields[24]

$$\langle \vec{R}_0, c|j\rangle=\left(-\frac{d}{dE_j}\,\mathrm{Re}[G(0,0,E_j)]\right)^{-1/2}. \tag{3b}$$

Equations (2) and (3) specify a solution which is exact, except for use of the effective-mass approximation. If V_l produces a bound state $|N_q^0\rangle$ of energy W_q and amplitude $|f_q|$ associated with the q conduction-band minima, whose energy is E_q (i.e., q stands for either Γ, X, or L), then Eq. (3a) can be written as

$$V_0\,\mathrm{Re}\left(\sum_q \frac{|f_q(0)|^2}{E_j-W_q+i\delta}+G_0(0,0,E_j)\right)=1\,. \tag{4}$$

The quantity G_0 represents the continuum contribution to the Green's function.

A detailed analysis of the solutions of Eq. (4) and a discussion of the prominent features of the model were performed previously.[24] Since we are interested principally in the bound-state solutions as in that work,[24] we also make the approximation[28] that $G_0(0,0,E_j)\cong\Lambda(E_j)$, the perfect-crystal Wannier-representation Green's function for E_j in the gap where

$$\Lambda(E)\equiv\frac{1}{N_0}\sum_{\vec{k}}\frac{1}{E-E_c(\vec{k})+i\delta}\,. \tag{5}$$

The quantity N_0 denotes the number of unit cells in the crystal.

At this point, the only information regarding the details of the potential used to model V_l which enters Eq. (4) is incorporated in the probabilities $|f(0)|^2$ of being located at $\vec{R}_n=0$ and the energies W. Given, therefore, a set of W we can completely describe a model potential by substituting the appropriate probabilities. Since it is not practicable to account for all model potentials, we simulate instead the effect of varying the model of V_l by multiplying $|f_q(0)|^2$ calculated for a chosen model potential (i.e., a square-well potential) by the same constant, dimensionless factor F for all q, where $F\equiv\int d^3r\,|f(\vec{r})|^2$. It has been shown[27] that a square-well potential has the smallest range and, therefore, the largest $|f(0)|^2$ of all model potentials which reproduce a given set of W. From wave-function normalization, we have $\sum_n |f(\vec{R}_n)|^2=1$, so that, for slowly varying $|f|^2$, $F=\Omega$, the numerical value of the volume of a unit cell. We define the strong coupling case, therefore, as corresponding to $F=\Omega$ and weak coupling is chosen arbitrarily as corresponding to $F=1.0$. The latter case was treated previously[24] and the former corresponds roughly to a properly normalized state. For simplicity in practice, we restrict ourselves to integral values of F, the highest being $F=40.0$ (i.e., $\Omega=[d(x)]^3/4=40.5$ Å^3 in GaP, where $d(x)=5.65-0.20x$ is the lattice constant in Å in Ga(As, P)).

In order to appreciate the effect of varying the strength of the coupling, we illustrate schematically in Fig. 2 the salient features of the solutions of Eq. (4) for the weak and strong coupling cases in direct Ga(As, P) (neglecting L). The dotted curves correspond to the left-hand side of Eqs. (3a) and (4) and the solid curve represents $V_0\mathrm{Re}G_0$. We let $G_0\simeq\Lambda$ (Ref. 28) so that $V_0\mathrm{Re}G_0(0,0,W_N)=1$ is the

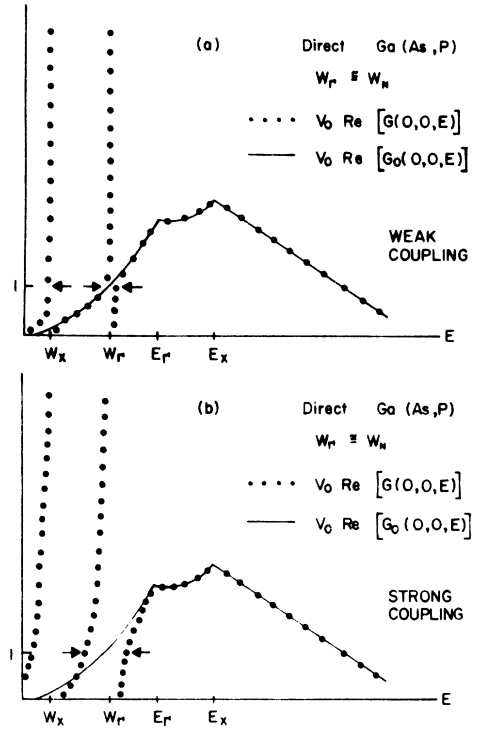

FIG. 2. Schematic illustration in direct Ga(As, P) of factors governing solution of the eigenvalue equation (4) for $W_\Gamma\cong W_N$ for (a) weak and (b) strong coupling. The quantities W_Γ and W_X denote energies of bound states produced by V_l associated with Γ and X, respectively, and W_N denotes the energy of the state arising from V_s. This figure shows how strong coupling modifies the solutions.

bound eigenvalue equation of the isoelectronic state $|N\rangle$ (energy W_N) arising from Eqs. (3a) and (4) when $V_I = 0$: In other words, we assume that the usual Koster-Slater short-range state[2,12-18] is unchanged except for the influence of the bound-state terms in Eq. (4). The features of the solutions of Eq. (4) shown in Fig. 2 have been discussed in detail elsewhere[24] for the weak-coupling case. For our present purposes, it is sufficient to observe that the presence of strong coupling causes the states to perturb each other strongly. Since the situation is much more complicated than for weak coupling,[24] we rely here on numerical calculations for insight. The general conclusions[24] regarding the properties of the solutions of Eq. (4) remain valid,[24] although details change.

As in a previous work,[24] we model V_I by a square well of depth U and radius a. For the lowest bound state associated with conduction-band minimum n, this model yields for weak coupling (i.e., $F = 1$)

$$f_n(0) = k_n\left(\frac{K_n/2\pi}{1+K_n a}\right)^{1/2}, \tag{6a}$$

$$K_n \equiv (2m_n\omega_n/\hbar^2)^{1/2}, \tag{6b}$$

$$k_n \equiv [2m_n(|U| - \omega_n)/\hbar^2]^{1/2}, \tag{6c}$$

$$\omega_n \equiv E_n - W_n. \tag{6d}$$

The subscript n refers to either Γ, X, or L (i.e., we consider L in Sec. II B), ω_n is the binding energy relative to minimum n, m_n symbolizes the effective conduction-band mass at n (i.e., $m_\Gamma/m_0 = 0.068 + 0.052x$, $m_X/m_0 = 0.35$, and $m_L/m_0 = 0.19$,[20,29] where m_0 is the free-electron mass).

We specify the Green's function Λ by a model[21,24,27] which describes the conduction band by ellipses of finite extent associated with the minima. This model yields the following result for Λ:

$$\Lambda(E) = \sum_i n_i \Lambda_i(E), \tag{7a}$$

$$\mathrm{Im}[\Lambda_i(E)] \equiv -\left(\frac{\Omega m_i}{2\pi\hbar^2}\right) s_i \Theta(E - E_i), \tag{7b}$$

$$\mathrm{Re}[\Lambda_i(E)] \equiv -\frac{m_i \Omega p_i}{\pi^2\hbar^2}\left[1 + \frac{r_i}{2}\ln\left|\frac{1-r_i}{1+r_i}\right|\Theta(E-E_i) - |r_i|\tan^{-1}\left(\frac{1}{|r_i|}\right)\Theta(E_i - E)\right], \tag{7c}$$

$$r_i \equiv s_i/p_i, \quad s_i^2 \equiv 2m_i(E - E_i)/\hbar^2. \tag{7d}$$

In Eqs. (7), Θ denotes the step function [i.e., $\Theta(y) = \frac{1}{2}(1 + y/|y|)$]. The quantity n_i represents the number of nonequivalent i minima (i.e., $n_\Gamma = 1$, $n_X = 3$, and $n_L = 4$), and p_i denotes a cutoff momentum whose magnitude is related to the number of states associated with i. In our calculations for Ga(As, P) we divide the Brillouin zone into three regions associated with the Γ, X, and L minima as in previous work.[13-16,21,24,25,27] These regions are, respectively, $0 \le Q_r \le 0.125$, $0.125 \le Q_r \le 0.50$, and $0.50 \le Q_r$, where $\vec{Q} \equiv \vec{k}d(x)/2\pi$ and r denotes a Cartesian coordinate. The resulting value for p_i is $p_i d(x) = (6\pi^2 V_{iQ}/n_i)^{1/3}$, where V_{iQ} is the volume in $\vec{Q}$ space of the i region. We derive $p_\Gamma d(x) = 0.974$, $p_X d(x) = 3.898$, and $p_L d(x) = 2.443$. The values of the energies of the minima which we use in our calculations are[1,19,20] in eV, $E_\Gamma = 1.514 + 1.174x + 0.186x^2$, $E_X = 1.977 + 0.144x + 0.211x^2$, and $E_L = 1.802 + 0.77x + 0.16x^2$.

In a previous article,[24] the weak-coupling version model was applied to N_Γ and N_X data[5] in Ga(As, P). Since there were only two experimental states observed and there are three parameters V_0, U, and a in the model, certain additional assumptions were made. First, it was assumed that the conventional[2] Koster-Slater model applied for $0.9 \lesssim x \lesssim 1.0$, so that V_I was zero. Second, in the region $x \lesssim 0.9$, a linear form for U and a constant for a were chosen, $U = U_0(1.4 - 1.15x)$ with $U_0 = -0.2623$ eV and $a = 24.8$ Å. This choice of parameters gave a good agreement with observed energies and a binding energy $E_X - W_X = 0.005$ eV in GaP.

The more complete set of data[10,23] illustrated in Fig. 1 allows us to relax these assumptions. Here we treat the whole range of x as one system and try to determine the extent to which the potential parameters can be extracted from the data for all x. As before,[24] we assume that all the composition dependence of the impurity potential resides in V_I and that V_s is the same in GaP and in the alloy. In principle, this separation is always possible. In practice, V_0 is taken to be x independent and the square-well parameters are allowed to vary: This is physically reasonable[25] but only an approximation to the true composition dependence of the nitrogen potential.

In Fig. 3, we exhibit energies calculated with the same potential parameters used previously[24] as a function of x for a series of coupling strengths F. The Koster-Slater parameter $V_0 = -2.677$ eV was calculated by adjusting the binding energy $E_X - W_N$ to 0.011 eV in GaP (see Ref. 30) in the eigenvalue equation[2,12-18,21,24]

$$V_0 = 1/\mathrm{Re}[\Lambda(W_N)]. \tag{8}$$

Figure 3(a) displays the energy eigenvalues W_X, W_Γ, and W_N calculated with these parameters. Also shown are the energies of the Γ, X, and L conduction-band minima, although we do not consider L in this section. In Figs. 3(b) to 3(d) we illustrate the effect of varying coupling strengths upon the final energy eigenvalues of Eq. (4). For weak coupling, as in Fig. 3(b), these energies are only

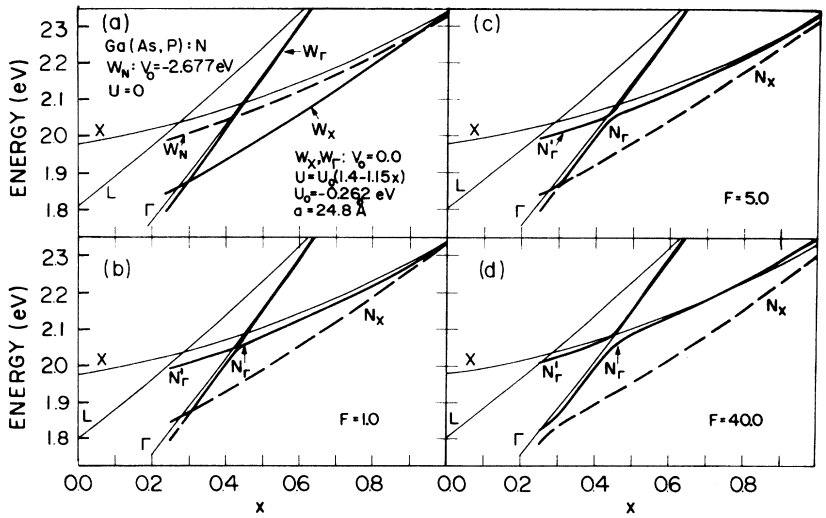

FIG. 3. Illustration of the effect of increasing coupling upon the eigenvalues of Eq. (4). (a) The uncoupled energies W_Γ, W_X ($V_s=0$), and $W_N(V_l=0)$ vs composition for the potential parameters indicated. (b) Eigenvalues of Eq. (4) for $F=1.0$ (weak coupling). (c) The same for $F=5.0$. (d) Eigenvalues of Eq. (4) for $F=40.0$ (strong coupling). The influence of L is ignored.

slightly changed from the decoupled eigenvalues W: Only in the vicinity of the Γ-X crossover is the hybridization splitting noticeable. As we increase the coupling in Figs. 3(c) and 3(d), we observe overall that the states repel one another. In the case of strong coupling, presented in Fig. 3(d), this has the effect that, for $x\cong 0.30$ and $x\cong 0.40$, there is a large splitting and a curvature in the energies, which is reflected in the data (e.g., see Fig. 1 and Ref. 6). The energy E_{N_X} is lowered throughout and, even more striking, the energy E_{N_Γ} of the next highest state is raised so much for $x \gtrsim 0.40$ that it is *pushed into the X continuum for large* x (i.e., $x\gtrsim 0.8$) so that there is only one bound state in this region. The energy $E_{N'_\Gamma}$ of the highest state is raised markedly for $x\lesssim 0.42$. It should be observed that those portions of energies which originated in W_Γ are only slightly affected by the coupling (i.e., E_{N_Γ} for $0.30\lesssim x\lesssim 0.40$ and $E_{N'_\Gamma}$ for $0.45\lesssim x$) because the small effective mass at Γ makes the bound-state term illustrated in Fig. 2 extremely local in energy.

The overall features of the systematics manifested in Fig. 3 are generally valid. It is clear, however, from Fig. 3(d), that the specific parameters employed in Fig. 3 do not give a good agreement with experimental data in the strong coupling regime. Nevertheless, we can exploit these systematics to learn how to choose parameters which improve the agreement.

In the region of x in Fig. 1 where three experimental lines are present, it is relatively easy to determine V_0, U, and a which produce good agreement with experiment [in practice, this involves solving the three nonlinear equations resulting from inserting the experimental energies into Eq. (4)]. In the region $x\gtrsim 0.47$, where only N_X is measured, such a procedure is not possible. Because of the systematics in Fig. 3(d), however, we can see that a balance must be struck between the results for $x=1.0$ and for $x\simeq 0.40$. If, at $x=1.0$, the square well is strong enough to produce a bound state associated with X, then $V_0\lesssim -2.677$ eV yields an E_{N_X} at $x=1.0$ which is much lower than E_X -0.011 eV because of the strong coupling. A value of $V_0>-2.677$ eV, however, produces a state N_Γ at $x\simeq 0.40$ which is much too high in energy to agree with data because of the slow variation of E_X with x. It appears, therefore, that the only viable alternative is to have at $x=1.0$, $W_X=E_X$ (i.e., no bound state) and $V_0=-2.677$ eV (which yields $E_{N_X}=0.011$ eV). This conclusion is borne out by the results of numerous computations.

Given the value of V_0 and W_X at $x=1.0$, we determine the other square-well parameters by assuming a to be constant, U to have a linear form as argued physically elsewhere,[24] and fitting to the experimental energies at $x\simeq 0.35$. The results of this procedure for $F=40.0$ are given in Fig. 4 where the values of the parameters are $U=(-0.378+0.338x)$ eV, and $a=24.8$ Å. In Fig. 4(a) we display as functions of x the uncoupled energies W_Γ, W_X, and W_N corresponding to these parameters as well as the energy W_L of the long-range state associated with L for later reference (since $m_L>m_\Gamma$, a bound state at Γ requires one at L). We present in Fig. 4(b), the results of the strong coupling of the W_Γ, W_X, and W_N shown in Fig. 4(a) and the com-

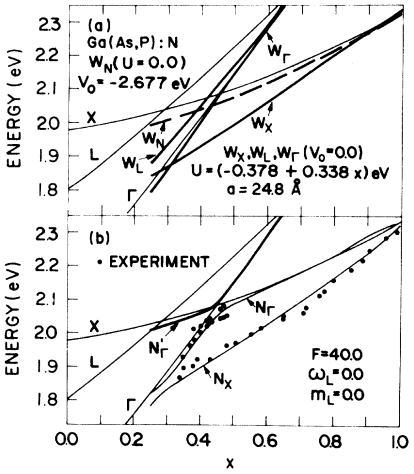

FIG. 4. (a) Concentration dependence of the uncoupled state energies corresponding to the parameters shown. For reference, the energy W_L of the long-range state associated with L is displayed. (b) Concentration dependence of the eigenvalues of Eq. (4) for the parameters in (a) and comparison with experiment (Refs. 5 and 10). The coupling is strong ($F=40.0$) and L is neglected. Bound-exciton energies of 0.01 eV were added to the experimental energies.

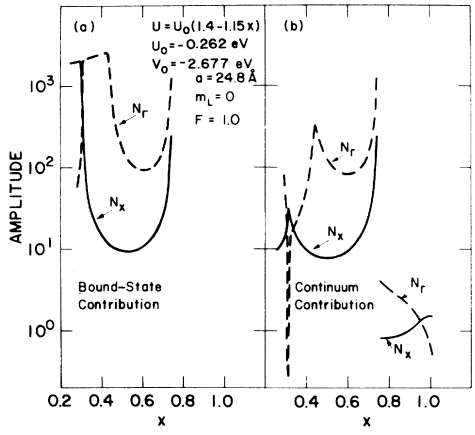

FIG. 5. (a) Magnitudes of the bound-state contributions to the $\vec{k}=0$ amplitudes of N_Γ and N_X for the parameters in Fig. 3(b) for $F=1.0$ (weak coupling). The divergence at $x\cong 0.8$ is an artifact of $W_\Gamma \to E_\Gamma$. Only bound states are considered. (b) Magnitudes of the continuum contributions to the $\vec{k}=0$ amplitudes corresponding to (a). The divergence at $x\cong 0.8$ exactly cancels the corresponding bound-state contribution. This figure emphasizes the importance of correctly calculating the continuum contribution.

parison with data[5,10] (i.e., the data points have been raised uniformly by 0.010 eV to account for bound-exciton energies[24]). The agreement between theory and experiment is quite good for all x. In particular, the picture in GaP resulting from this study is consistent with the usual one,[1,2,12-18] that is, the observed nitrogen state is produced mainly by the Koster-Slater potential interacting with the continuum, since $W_X=E_X$ at $x=1.0$. Moreover, the radius $a=24.8$ Å is consistent with the long-range nature of the potential.

The luminescence of a state $|j\rangle$ is most easily characterized by the momentum amplitude at $\vec{k}=0$, which, in this theory[6,24] is given by

$$\langle \vec{k}=0, c|j\rangle = V_0 G(\vec{k}=0,\vec{R}_0,E_j)\langle \vec{R}_0, c|j\rangle , \tag{9a}$$

$$G(\vec{k}=0,\vec{R}_0,E) \equiv \frac{1}{\sqrt{N_0}}\sum_q \frac{C_q(0)f_q^*(0)}{E-W_q+i\delta} + G_0(\vec{k}=0,\vec{R}_0,E), \tag{9b}$$

$$G_0(\vec{k},\vec{R}_0,E) \equiv \frac{1}{\sqrt{N_0}}\sum_m e^{-i\vec{k}\cdot\vec{R}_m} G_0(\vec{R}_m,\vec{R}_0,E), \tag{9c}$$

$$C_q(\vec{k}) \equiv \sum_m e^{-i\vec{k}\cdot\vec{R}_m} f_q(\vec{R}_m), \tag{9d}$$

where the sum in Eq. (9b) is over bound states of V_l, $\vec{R}_0=0$, $|\vec{k},c\rangle$ is a conduction-band Bloch state, and our notation is consistent with that in Eqs. (1)–(5).

From Eqs. (9) we observe that we need to calculate the Green's function defined in Eq. (9b). From the localization in $\vec{k}$ space of the bound states of V_l, we can write[24] for bound $|j\rangle$:

$$G(\vec{k}=0,\vec{R}_0,E_j) \cong \frac{1}{\sqrt{N_0}}\,\frac{C_\Gamma(0)f_\Gamma^*(0)}{E_j-W_\Gamma} + G_0(\vec{k}=0,\vec{R}_0,E_j), \tag{10a}$$

where, in the square-well model,[24] we have from Eqs. (6):

$$C_\Gamma(0) = 2/\alpha_\Gamma K_\Gamma f_\Gamma(0) a, \tag{10b}$$

$$\alpha_\Gamma \equiv 1/a(K_\Gamma^2+k_\Gamma^2)^{1/2}. \tag{10c}$$

In order to emphasize the importance of accounting properly for the continuum contribution to the luminescence embodied in G_0 in Eq. (10a), we present the bound-state contribution [corresponding to the first term on the right-hand side of Eq. (10a)] to $\langle \vec{k}=0\,|j\rangle$ in Fig. 5(a) as a function of x for the E_j of Fig. 3(b) which are in the gap and we drop the factor $N_0^{-1/2}$. The parameters are the same as for Fig. 3(b) (i.e., weak coupling). Besides the structure near $x\cong 0.30$ and $x\cong 0.40$ resulting from hybridization predicted previously,[24] there is a divergence for $x\cong 0.75$ which is an artifact of the fact that $W_\Gamma \to E_\Gamma$ at these compositions. From Eqs. (6) and (10), this divergence is obvious and results from the great spatial extent of a bound state with small binding energy.

For the model under consideration, we can calculate[31] this contribution with a liberal application of scattering theory.[32] We report the details of the calculation elsewhere[31] and concentrate here on the result for $E_j < E_\Gamma$:

$$G_0(\vec{k}=0,\vec{R}_0,E_j)\cong A\left(\frac{1}{\cos(1/\alpha_\Gamma)(E_j-E_\Gamma)}+\frac{[\sin(\gamma a)-\gamma a\cos(\gamma a)]\,[(E_\Gamma-E_j)(E_j-E_\Gamma-U)]^{-1/2}}{\alpha_\Gamma^2\{[\gamma a\cos(\gamma a)]^2-[sa\sin(\gamma a)]^2\}}\right.$$
$$\left.-\frac{\Theta(2/\pi-\alpha_\Gamma)}{\alpha_\Gamma K_\Gamma a(E_j-W_\Gamma)}-\frac{\Theta(\alpha_\Gamma-2/\pi)}{\alpha_\Gamma K_R a(|E_R-E_\Gamma|-E_\Gamma+E_j)}\right), \tag{11a}$$

$$s^2\equiv\frac{2m_\Gamma}{\hbar^2}(E_\Gamma-E_j),\quad \gamma^2\equiv(\alpha_\Gamma a)^{-2}-s^2, \tag{11b}$$

$$K_R^2\equiv\frac{2m_\Gamma}{\hbar^2}|E_R-E_\Gamma|. \tag{11c}$$

The parameters K_Γ and α_Γ are defined in Eqs. (6b) and (10c), respectively, and A is a normalization constant equal to $1/\sqrt{N_0}$ and $[\Omega/(2\pi)^3]^{1/2}$ for discrete and continuum normalization, respectively. The quantity E_R is a resonance energy defined for $2/\pi\leq\alpha_\Gamma\leq 1$ (i.e., $\alpha_\Gamma\leq 2/\pi$ is the bound-state condition) by

$$\alpha_\Gamma K_R a=\sin(K_R a), \tag{11d}$$

where $\cos(K_R a)>0$, and for $1\leq\alpha_\Gamma$ by

$$\alpha_\Gamma|K_R a|=\sinh(|K_R a|),\quad \mathrm{Re}K_R=0. \tag{11e}$$

The absolute magnitude of the continuum contribution to $\langle\vec{k}=0\,|j\rangle$ is plotted in Fig. 5(b) as a function of x for the same parameters as in Fig. 5(a) and we ignore the factor of A as we do in other figures. The first term in Eq. (11a) derives from the unperturbed conduction-band continuum. The third term, which reflects bound-state poles in the scattering amplitude,[31,32] combines with the first to produce the divergent structure at $x\cong 0.75$ in Fig. 5(b) (i.e., $\alpha_\Gamma\lesssim 2/\pi$). This structure cancels exactly the corresponding structure in the bound-state contribution in Fig. 5(a). For $\alpha_\Gamma\gtrsim 2/\pi$, the first term changes sign and cancels the divergent structure in the fourth term, which originates from the presence of scattering resonances, leaving the smoothly varying second term as dominant for $x\gtrsim 0.75$, as illustrated in Fig. 5(b). The structure for $x\cong 0.3$ and $x\cong 0.4$ reflects the hybridization displayed in Fig. 3(b).

In Fig. 6(a), we present the total $|\langle\vec{k}=0\,|j\rangle|$ versus composition for the bound states N_X and N_Γ in Fig. 3(b). The parameters here are the same as in Figs. 3(b) and 5 (i.e., $F=1.0$). It is clear that there is no divergent structure in the total amplitude and that a full calculation reflects results derived earlier.[24] Both states are sharply enhanced as they approach the respective hybridization regions of x. In the region $0.5\lesssim x\lesssim 0.9$, the N_X amplitude is larger than that calculated before[24] because of our superior treatment of the continuum contribution. Also given in Fig. 6(a) is the ordinary band structure enhancement (BSE) amplitude for N_X state, defined as

$$N_X(\mathrm{BSE})=\frac{[-\Lambda'(E_{N_X})]^{-1/2}}{E_{N_X}-E_\Gamma}, \tag{12}$$

where the prime denotes the derivative. From this comparison, it is clear that, in this model a much larger enhancement is produced by the strong luminescence of the state of V_i associated with Γ than by the unperturbed conduction band as in Eq. (12).

In Fig. 6(b), we give the total amplitude $|\langle\vec{k}=0\,|j\rangle|$ corresponding to the bound-state energies of Fig. 3(d) [i.e., Fig. 6(b) is the strong coupling version of Fig. 6(a)]. Although the enhancement illustrated in Fig. 6(a) is still present, the sharpness of the x variation is reduced in the regions of hybridization. Besides details of the variation, which derive from the spectrum in Fig. 3(d) and the normalization factor in Eq. (3b), the most important result is that strong coupling makes the amplitudes much closer in magnitude: Strong coupling

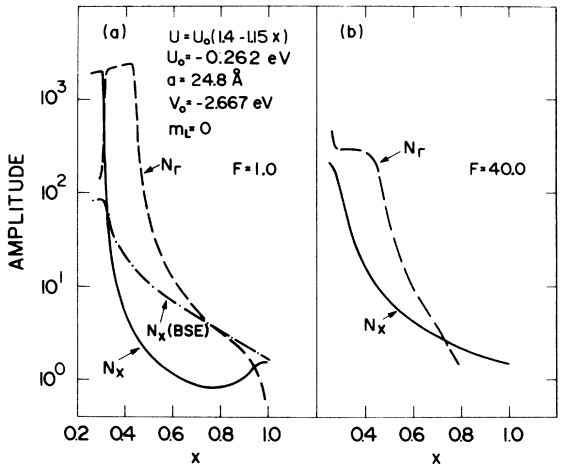

FIG. 6. (a) Magnitudes of the total $\vec{k}\simeq 0$ amplitudes corresponding to the parameters of Fig. 5. The structure for $x\simeq 0.8$ is smooth and only the hybridization enhancement at $x\simeq 0.3$ and $x\simeq 0.4$ remains. Illustrated is the expected band-structure-enhancement term of Eq. (12) for N_X calculated for weakly coupled ($F=1.0$) energies. (b) Strong coupling ($F=40.0$) version of (a). Hybridization enhancement is smaller and the N_Γ and N_X amplitudes are much closer in value than in (a).

actually increases the value of the N_X amplitude relative to the weak-coupling case. Note that there is no N_Γ state for $x > 0.8$ in Fig. 6(b).

The total N_X and N_Γ bound-state amplitudes for the potential parameters in Fig. 4, which produce agreement with experimental energies for $F = 40.0$, are presented in Figs. 7(a) for $F = 1.0$ and 7(b) for $F = 40.0$ as functions of x. The general conclusions resulting from our discussion of Fig. 6 remain unchanged. Strong coupling reduces the sharpness of the hybridization structure and brings the N_Γ and N_X amplitudes closer in magnitude than in the $F = 1.0$ case. In Fig. 7(b), it is clearly indicated that N_Γ enters the X continuum for $x \gtrsim 0.75$, and that the N_X amplitude is larger than the N_Γ for $x \gtrsim 0.70$.

B. Influence of the L minimum

In this section, we examine the influence of the L conduction-band minimum upon the energies and momentum amplitudes of the eigenstates of Eqs. (2)–(4) in the case of strong coupling. We find that, although the energies are sensitive to the presence of L, the momentum amplitudes change little. Parameters extracted from experiment are in accord with the long-range character of the model.

In Fig. 8, we present the calculated energies as functions of x, corresponding to the potential parameters of Figs. 4(b) and 7(b) resulting from consideration of L— these parameters produce strongly coupled energies which agree with experiment when we consider only Γ and X (i.e., see Fig. 4). Figure 8(b) displays the energies produced by including L in the conduction-band density of states in Eq. (7) only without accounting for the bound state produced by V_l, which is associated with the L minima shown in Fig. 4(a). Upon comparing with Fig. 4(b), we see that the major effect is that of lowering all of the energies and increasing their variation with x, especially for N_Γ for $x \gtrsim 0.4$ and N_Γ' for $x \lesssim 0.4$.

The effects of including the L bound state [which is shown in Fig. 4(a)] are presented in Fig. 8(b) for the same parameters. Comparing with Fig. 4(a), we observe that this spectrum involves an additional hybridization for $x \lesssim 0.4$ between the isoelectronic state $|N\rangle$ and the long-range state associated with L, besides the ones discussed heretofore.[24] The overall effect is that $E_{N_\Gamma'}$ is greatly lowered for $x \lesssim 0.4$ because of this strong hybridization (i.e., $F = 40.0$). The other states N_Γ and N_X are much less influenced.

The momentum amplitudes corresponding to the bound-state energies of Figs. 8(a) and 8(b) are given as functions of x in Figs. 9(a) and 9(b), respectively. Our previous conclusions regarding the effects of strong coupling upon the enhancement in the regions of hybridization and upon the closeness in magnitude of the N_Γ and N_X amplitudes are supported. The difference from Fig. 7(b) can be attributed to the changes in the energy spectrum pro-

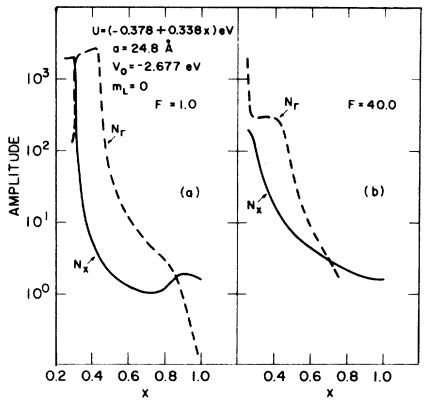

FIG. 7. (a) Magnitudes of the total $\vec{k} = 0$ amplitudes of N_X and N_Γ as functions of x for the parameters of Fig. 4 in the weak-coupling ($F = 1.0$) case when L is neglected. Only bound states are treated. (b) Strong-coupling ($F = 40.0$) version of (a). Hybridization enhancement and the difference in magnitudes of the N_Γ and N_X amplitudes are reduced. This case corresponds to the energies presented in Fig. 4(b). Note that N_Γ is not bound for $x \gtrsim 0.75$.

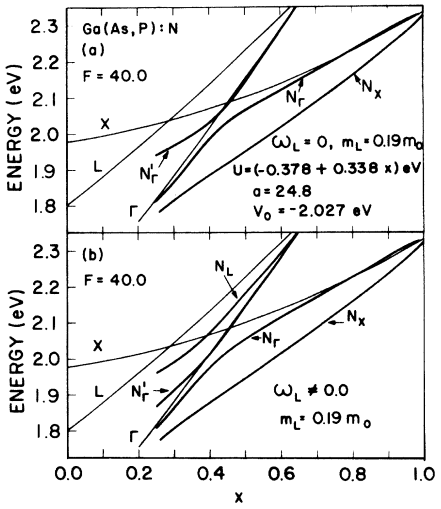

FIG. 8. (a) Concentration dependence of energies of Γ, X, L, and the states predicted by the theory when the L minimum is included only in the conduction-band density of states. The parameters correspond to those in Figs. 4 and 7 and strong coupling ($F = 40.0$) is considered. The effect of L is to reduce the energies of all the nitrogen states. (b) The same as (a) except that the long-range state associated with L is also considered. Note the extra hybridization of the N_Γ' and N_L states for $x \lesssim 0.4$. The effect of the L bound state on the other states is small.

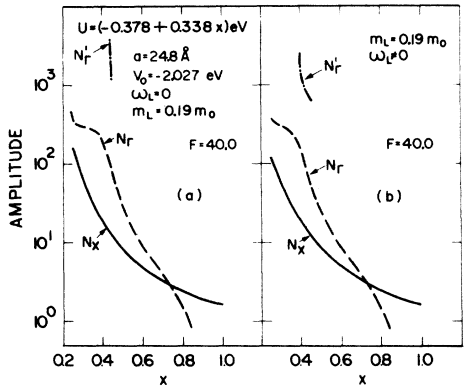

FIG. 9. (a) x dependence of the magnitudes of the total $\vec{k}=0$ amplitudes corresponding to the bound energies in Fig. 8(a). (b) x dependence of amplitudes corresponding to bound states of Fig. 8(b). The dominant effect of L is in the density of states.

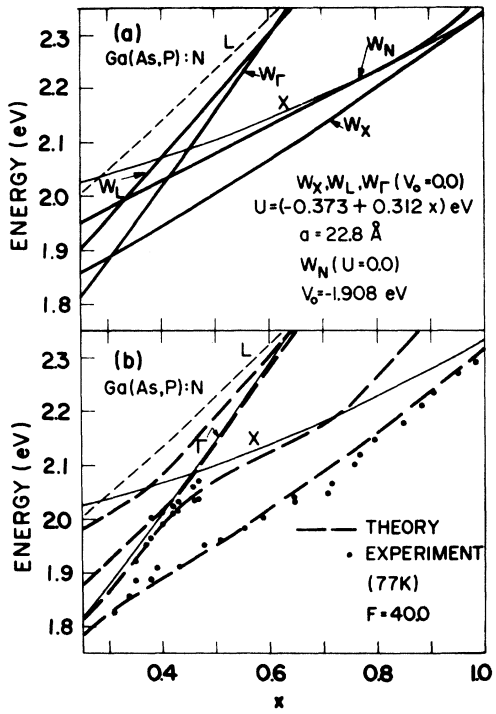

FIG. 10. (a) Concentration dependence of the uncoupled state energies for the case when L is considered fully. The parameters were chosen to give good agreement with experiment at $x\simeq 0.4$ and $x=1.0$ for $F=40.0$. (b) Concentration dependence of the eigenvalues of Eq. (4) corresponding to the parameters in (a). Bound-exciton energies of 0.01 eV were subtracted from the calculated energies. Experimental data from Refs. 10 and 23 are presented also.

duced by L. From comparing Figs. 9(a) and 9(b), it is notable that the presence of the L bound state has only a small effect on the N_Γ and N_X amplitudes. Also illustrated is the amplitude of N_Γ'—of all the cases we discuss in this paper, this is the only one in which N_Γ' is bound over a significant region of x. Proper treatment of the luminescence of resonance states within this theory is outside the scope of this article and is treated elsewhere.[31] The effect of the long-range state upon N_Γ' is manifested clearly.

From comparing Fig. 8 with Fig. 4, it is apparent that inclusion of the effects of the L minima destroys agreement with the data. In order to determine a set of potential parameters in this case (i.e., $F=40.0$), we insert three experimental energies for $x\cong 0.39$ into Eq. (4), forming a set of three nonlinear equations in V_0, U, and a. The V_0 and a so determined are held constant and U is adjusted at $x=1.0$ to give the single observed state of energy $E_X-0.011$ eV.[1,13-18,21,24] The results of this procedure are $V_0=-1.908$ eV, $U=(-0.373+0.312x)$ eV, and $a=22.8$ Å. Note that, even when the effect of L is included, the parameters derived are consistent with the long-range nature of the potential.

In Fig. 10(a), we display the energies of the uncoupled states resulting from this choice of parameters. It is interesting that, because of the rapid x variation introduced by the density of states at L, the Koster-Slater parameter extracted from the data is too weak to produce a bound $|N\rangle$ at $x=1.0$. The strongly coupled energies resulting are presented in Fig. 10(b), where they are compared with the data (i.e., a bound exciton energy of 0.010 eV is subtracted from the calculated energies). The general conclusions reached earlier are borne out here and agreement with experiment is very good.

Bound-state momentum amplitudes corresponding to the parameters in Fig. 10 are given as functions of x in Fig. 11(a) for weak coupling and in Fig. 11(b) for strong coupling. Our previous conclusions regarding the effect of strong coupling and the x variation are supported. Here, the N_Γ state enters the X continuum for $x\gtrsim 0.6$ and the N_Γ and N_X amplitudes are of roughly the same magnitude for $x\gtrsim 0.50$.

III. COMPARISON WITH EXPERIMENT

In Sec. II, we concentrated upon studying the degree to which calculated energies could be brought into agreement with experiment and the systematics of the energies and luminescence (as incorporated in the $\vec{k}=0$ momentum amplitudes) of the states predicted by the Kleiman[6,24] theory. Here we devote our attention to examining the degree of agreement with luminescence measurements of the properties of the states whose energies we have

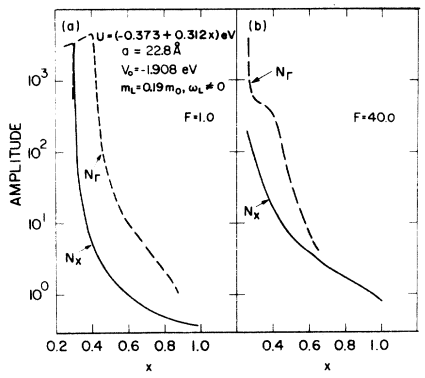

FIG. 11. (a) Concentration dependence of the $\vec{k}=0$ amplitudes, corresponding to the weakly coupled ($F=1.0$) bound-state eigenvalues of Eq. (4) for the parameters of Fig. 10 (i.e., L is taken fully into account). (b) The same as (a) except for strong coupling ($F=40.0$). N_Γ is resonant for $x \gtrsim 0.7$.

already determined to be in accord with experiment.

In Fig. 12, we present the ratios of the N_Γ and N_X $\vec{k}=0$ probabilities as functions of x for the strong-coupling cases where L is not considered [i.e., Fig. 12(a)] and where it is [i.e., Fig. 12(b)]. These figures correspond, respectively, to the amplitides in Figs. 7(b) and 11(b). For our present purposes, we note only that the ratio peaks at $x \simeq 0.45$ in Fig. 12(a) and at $x \simeq 0.40$ in Fig. 12(b). Luminescence measurements for nitrogen-implanted samples indicate a peak in this ratio at $x \simeq 0.37$.[25] The agreement is good especially in view of the fact that the potential parameters were determined from data for as-grown samples.[5,10] The results of this comparison would seem to indicate the importance of accounting for L properly.[19,20]

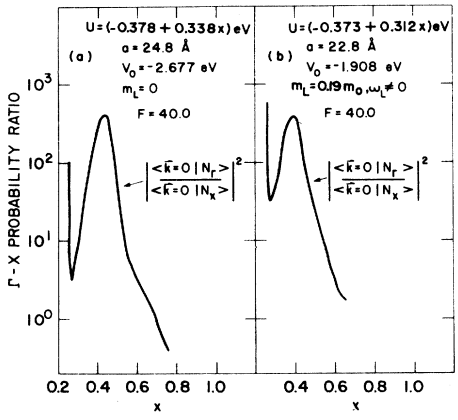

FIG. 12. (a) Concentration dependence of N_Γ to N_X $\vec{k}=0$ probability ratio for the case when L is neglected and the strongly coupled ($F=40.0$) energies are adjusted to the data (i.e., the parameters correspond to Figs. 4 and 7). (b) The same as (a) except that the parameters (see Figs. 10 and 11) are derived when L is taken into account. Data on nitrogen-implanted material (Ref. 25) indicate a maximum at $x \simeq 0.37$.

Pressure measurements[8] of the normalized electroluminescence intensity of N_X at $x=0.65$ (i.e., solid circles) and N_Γ at $x=0.48$ (i.e., triangles) are presented in Fig. 13. Also illustrated are the respective normalized $\vec{k}=0$ probabilities for the two cases treated previously [i.e., Figs. 7(b) and 11(b)]. In converting from x to pressure we use the value[8] $dx/dp \sim 1.1\%$/kbar. The agreement with experiment is quite good in both cases, although there is little to favor the inclusion of L. These results reflect earlier[8] ones.

In Fig. 14 we compare N_X lifetime versus x measurements[26] with lifetimes calculated for the strong-coupling cases when L is considered (i.e., broken line) and when it is not (i.e., solid line). The theoretical lifetimes are presumed to vary as the inverse of the $\vec{k}=0$ probability of N_X and are normalized to the experimental value[33] in GaP. The agreement is quite good in both cases and would seem to support the exclusion of L from consideration. The unusual variation in the theoretical lifetime without L for $x \lesssim 1.0$ in Fig. 14 reflects the fact that the Koster-Slater and long-range X state interact strongly at a composition $x<1$ (i.e., in this case, there is no bound state of V_i in GaP).

IV. CONCLUSIONS

In this article, we examined the systematics governing the long-range, short-range, or Kleiman[6,24] theory of the nitrogen isoelectronic impurity in Ga(As, P), and the extent to which states arising from the theory could be brought into agreement with available data.[3-10,25,26] In Sec. II,

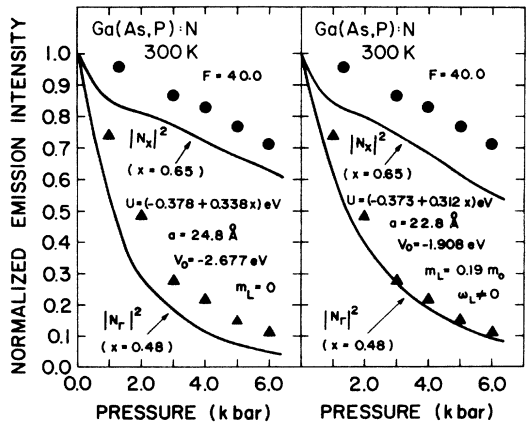

FIG. 13. (a) Pressure dependence for the states shown corresponding to the case in Fig. 4(b). The data is from Ref. 8. (b) Pressure dependence corresponding to Fig. 10(b). The data is from Ref. 8.

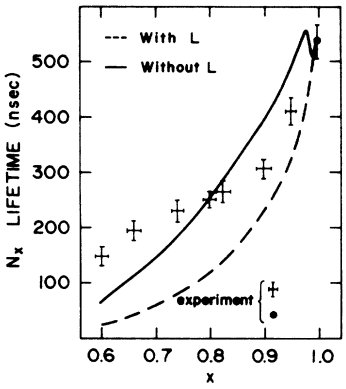

FIG. 14. Concentration dependence of experimental lifetimes (Ref. 26) and the inverse of the N_X $\vec{k}=0$ probabilities corresponding to Fig. 4(b) (i.e., solid line) and Fig. 10(b) (broken line). Theory is normalized to experiment in GaP (Ref. 33).

we discussed the influence of strong coupling among the constituent states arising from either the long-range or the short-range part of the potential and the influence of the L conduction-band minima. Some of the general consequences of the strong coupling (as illustrated in Fig. 3) are curvatures in the calculated energies as functions of composition at $x \simeq 0.3$ and $x \simeq 0.4$ (the regions of hybridization) and raising of the N_Γ energy above the X-band edge (i.e., resonance) for large x, so that only N_X is observable at these compositions. Potential parameters which are consistent with the long-range nature of the model (i.e., the square-well radius ~20–25 Å) produce good agreement with experimental data as in Figs. 4 and 10.

In calculating luminescence properties, in particular the $\vec{k}=0$ momentum amplitudes, both the bound state and continuum contributions must be calculated properly in order to avoid unphysical structure in the total amplitude as summarized in Figs. 5 and 6. In general, the presence of strong coupling reduces the enhancement corresponding to weak coupling produced as $E \to W_\Gamma$, the energy of the strongly luminescent state derived from the long-range potential associated with the Γ minima. Even for strong coupling, this enhancement is larger than BSE.[1,2,12-18] In addition, strong coupling greatly decreases the difference in magnitudes of the $\vec{k}=0$ amplitudes of N_Γ and N_X (e.g., Figs. 7 and 11). This could explain[24] the absence of observation of N_Γ for $x \gtrsim 0.5$.

The highest energy state N_Γ' predicted by the theory is bound in only exceedingly small range of x for the potential parameters derived from experiment. Discussion of the influence of N_Γ' on the luminescence awaits a treatment[31] of resonant states in this theory.

It is only in the description of the states in GaP that inclusion of the L minimum[19,20] has any major effect. When we neglect L in this theory, the observed state in GaP must be attributed to the Koster-Slater model for consistency—there can be no long-range bound states. Consideration of L, however, requires that the GaP state arise from a long-range state with a resonant excited state derivable from the Koster-Slater model. This separation into long-range and Koster-Slater states is somewhat arbitrary, since the strong coupling causes each final state to have a mixture of the uncoupled states.[24] Nevertheless, inclusion of the effects of L (Refs. 19, 20) suggests that the long-range part of the potential is important in GaP, and that an excited state is present.[34]

Finally, in Sec. III we show that the theoretical states resulting from inclusion and from exclusion of the effects of L produce good agreement with all available data.[8,25,26] There is, therefore, little in the nitrogen data to indicate the importance of including L.

In brief, we have shown that the Kleiman theory[6,24] can be put into good agreement with the data without inconsistencies in contrast[27] to intermediate-range models.[25]

ACKNOWLEDGMENTS

We would like to thank FAPESP, CNPq, and FINEP of Brasil for their support.

[1]M. G. Craford and N. Holonyak, Jr., in *Optical Properties of Solids: New Developments*, edited by B. O. Seraphin (North-Holland, Amsterdam, 1975), Chap. 5.
[2]P. J. Dean, J. Lumin. 1/2, 398 (1970).
[3]D. J. Wolford, B. G. Streetman, R. J. Nelson, and N. Holonyak, Jr., Solid State Commun. 19, 741 (1976).
[4]D. J. Wolford, B. G. Streetman, W. Y. Hsu, J. D. Dow, R. J. Nelson, and N. Holonyak, Jr., Phys. Rev. Lett. 36, 1400 (1976).
[5]R. J. Nelson, N. Holonyak, Jr., J. J. Coleman, D. Lazarus, W. O. Groves, D. L. Keune, M. G. Craford, D. J. Wolford, and B. G. Streetman, Phys. Rev. B 14, 685 (1976).
[6]G. G. Kleiman, R. J. Nelson, N. Holonyak, Jr., and J. J. Coleman, Phys. Rev. Lett. 37, 375 (1976).
[7]R. J. Nelson, N. Holonyak, Jr., J. J. Coleman, D. La-

zarus, D. L. Keune, W. O. Groves, and M. G. Craford, Phys. Rev. B 14, 3511 (1976).
[8]R. J. Nelson, N. Holonyak, Jr., J. J. Coleman, D. Lazarus, D. L. Keune, A. H. Herzog, W. O. Groves, and G. G. Kleiman, Appl. Phys. Lett. 29, 615 (1976).
[9]R. J. Nelson and N. Holonyak, Jr., Solid State Commun. 20, 549 (1976).
[10]N. Holonyak, Jr., R. J. Nelson, J. J. Coleman, P. D. Wright, D. Finn, W. O. Groves, and D. L. Keune, J. Appl. Phys. 48, 1963 (1977).
[11]G. F. Koster and J. C. Slater, Phys. Rev. 95, 1167 (1954).
[12]R. F. Faulkner, Phys. Rev. 175, 991 (1968).
[13]D. R. Scifres, N. Holonyak, Jr., C. B. Duke, G. G. Kleiman, A. B. Kunz, M. G. Craford, W. O. Groves, and A. H. Herzog, Phys. Rev. Lett. 27, 191 (1971).
[14]D. R. Scifres, H. M. Macksey, N. Holonyak, Jr., R. D. Dupuis, G. W. Zack, C. B. Duke, G. G. Kleiman, and A. B. Kunz, Phys. Rev. B 5, 2206 (1972).
[15]C. B. Duke, D. L. Smith, G. G. Kleiman, H. M. Macksey, N. Holonyak, Jr., R. D. Dupuis, and J. C. Campbell, J. Appl. Phys. 43, 5134 (1972).
[16]G. G. Kleiman, J. Appl. Phys. 47, 180 (1976).
[17]M. Altarelli, Phys. Rev. B 11, 5031 (1975).
[18]J. J. Coleman, N. Holonyak, Jr., A. B. Kunz, W. O. Groves, D. L. Keune, and M. G. Craford, Solid State Commun. 16, 319 (1975).
[19]D. E. Aspnes, C. G. Olson, and D. M. Lynch, Phys. Rev. Lett. 37, 766 (1976).
[20]D. E. Aspnes, Phys. Rev. B 14, 5331 (1976).
[21]G. G. Kleiman and M. Fracastoro-Decker, Phys. Rev. B 17, 924 (1978).
[22]The symbols, Γ, X, and L denote Γ_6^c, X_6^c, and L_6^c, respectively.
[23]N. Holonyak, Jr. (private communication).
[24]G. G. Kleiman, Phys. Rev. B 15, 802 (1977).
[25]W. Y. Hsu, J. D. Dow, D. J. Wolford, and B. G. Streetman, Phys. Rev. B 16, 1597 (1977).
[26]J. Chevallier, H. Mariette, D. Diguet, and G. Poibland, Appl. Phys. Lett. 28, 375 (1976).
[27]G. G. Kleiman, Phys. Rev. B 19, 3198 (1979).
[28]Implicit in the approximation $G_0 \simeq \Lambda$ is the assumption that we are dealing with E_j sufficiently deep that G_0 is insensitive to details of the conduction-band density of states.
[29]A. Onton and R. C. Taylor, Phys. Rev. B 1, 2587 (1970); C. Alibert, G. Bordure, A. Laugier, and J. Chevallier, *ibid.* 6, 1301 (1972).
[30]This procedure leads to a slightly different V_0 than used in Ref. 24 because the conduction-band parameters used here are slightly improved.
[31]G. G. Kleiman and M. Fracastoro-Decker (unpublished).
[32]M. L. Goldberger and K. M. Watson, *Collision Theory* (Wiley, New York, 1964).
[33]J. D. Cuthbert and D. G. Thomas, Phys. Rev. 154, 763 (1967).
[34]E. Cohen and M. D. Sturge, Phys. Rev. B 15, 1039 (1977).